Photoluminescence study of the exciton dynamics at PTCDA/noble-metal interfaces

Klaus Stallberg,* Andreas Namgalies, and Ulrich Höfer
Fachbereich Physik und Zentrum für Materialwissenschaften, Philipps-Universität, 35032 Marburg, Germany

(Received 2 October 2018; revised manuscript received 29 January 2019; published 8 March 2019)

Charge and energy transport across organic/metal interfaces play a decisive role for the functionality of organic semiconductor devices. As well-defined model systems for such heterointerfaces, we consider thin films of the organic semiconductor perylene-tetracarboxylicacid-dianhydride (PTCDA) deposited on the single-crystalline (111)-surfaces of the noble metals silver and gold. By means of time-resolved photoluminescence we investigate the exciton dynamics of these systems in the energy and time domain. Systematic variation of the PTCDA film thickness enables us to follow the exciton relaxation rates as a function of the molecule–metal separation from several nanometers down to a few angstroms. Spatially localized excitations, such as excimers, are found to relax by nonradiative energy transfer to the metal. In contrast, the relaxation of charge-transfer (CT) excitons can be explained by exciton diffusion and subsequent annihilation at the organic/metal interface. Both mechanisms are found to be much more efficient on Ag(111) than on Au(111). For excimers, the faster relaxation on the silver substrate presumably involves the excitation of intraband transitions inside the metal. The higher relaxation rate of CT excitons is explained in terms of enhanced charge transfer across the PTCDA/Ag(111) interface, which is mediated by the electronic interface state inherent to this organic/metal interface.

DOI: 10.1103/PhysRevB.99.125410

I. INTRODUCTION

Organic semiconductors are nowadays widely employed, e.g., as organic light-emitting diodes (OLEDs) in displays of consumer-electronics devices or in organic solar cells. Despite these prosperous applications, the physical principles that underlie transport and relaxation of optical excitations within organic semiconductors are still a subject of intensive research. In this context, films of essentially planar π-conjugated molecules, such as perylene-tetracarboxylicacid-dianhydride (PTCDA), have emerged as invaluable model systems as they allow us to observe and analyze such processes within a well-defined and well-characterized environment without the chemical and structural complexity of actual devices. The growth of PTCDA has extensively been investigated for various substrates and the molecular structure of thin PTCDA films is precisely known in the meantime [1–14]. While at low temperatures the films predominantly grow in the β-configuration of crystalline PTCDA, at elevated temperatures above 350 K the α phase prevails, whereas at room temperature both phases coexist. Under appropriate conditions, PTCDA films grow layer by layer on single-crystalline metal surfaces with only little surface roughness [5–7,14]. This enables the fabrication of PTCDA films with well-defined film thicknesses.

We choose the (111)-oriented single-crystalline surfaces of the noble metals silver and gold as substrates, as they represent prototypical systems with strong and weak electronic molecule–metal interaction, respectively. While PTCDA molecules are comparatively loosely bound on the Au(111) surface, PTCDA chemisorbs on Ag(111) accompanied by charge transfer from the metal to the molecule. As a consequence, the former lowest unoccupied molecular orbital (F-LUMO) of PTCDA becomes partially filled, altering the electronic and optical properties of PTCDA in the first molecular layer. Most noteworthy, an unoccupied electronic interface state is inherent to the PTCDA/Ag(111) interface, which is absent in the case of PTCDA/Au(111) [11,15].

The optical properties of organic semiconductors are largely determined by the formation of excitons, which can be excited directly by absorption of light or indirectly as a product of relaxation processes of photoexcited molecules. In addition to Frenkel excitons, which are situated at individual molecules, in layered systems the overlapping π-orbitals of molecules in adjacent layers facilitate the formation of charge-transfer (CT) excitons between neighboring molecules [13,16]. Especially in systems where excitons strongly interact with the crystal lattice, CT excitons tend to stabilize via self-trapping and even form excimers [13,17,18]. The formation and relaxation of excitons in films of PTCDA have been addressed in numerous publications where they mainly were studied by means of time-integrated photoluminescence (PL) [4,13,18–21]. While time-resolved PL data exists for submonolayers of MePTCDI on quartz [22], for PTCDA, time-resolved experiments have been performed exclusively with bulk crystals so far [23,24]. Here, we present a time-resolved PL study of the exciton dynamics in thin PTCDA films with systematically varied film thickness. Applying a sort of tomography approach, we are able to access the relaxation dynamics of excitons in individual layers of an organic film. Analyzing the PL signals in the energy and time domain, we reveal different relaxation mechanisms for the different kinds of excitons. More specifically, we demonstrate that near-field interaction with the conduction electrons of the supporting metal is the dominant relaxation pathway for

*klaus.stallberg@physik.uni-marburg.de

excimers or self-trapped excitons in metal-supported PTCDA films. In contrast to these localized excitations, CT excitons are able to diffuse through the organic film and annihilate at the organic/metal interface by creation of hot electrons inside the metal. Especially in the case of a Ag(111) substrate, this process is significantly enhanced, presumably due to the presence of the metal–organic interface state [11,15,25] of the PTCDA/Ag(111) system.

II. EXPERIMENTAL METHODS AND SAMPLE PREPARATION

Sample preparation as well as all experiments were conducted inside an ultrahigh vacuum (UHV) chamber with a base pressure below 10^{-10} mbar. Clean and structurally well-defined Ag(111) and Au(111) single-crystal surfaces were prepared by cycles of argon ion sputtering ($10\,\mu$A mm^{-2}, 700 V) for 15 min at a sample temperature of $T_S = 373$ K and by subsequent annealing at $T_S = 773$ K for 5 min. The cleanliness and structural order of both surfaces was confirmed by x-ray photoelectron spectroscopy (XPS), low-energy electron diffraction (LEED), and two-photon photoemission (2PPE). PTCDA films were grown on the metal substrates at 273 K with rates between 1 Å and 1.5 Å per min by thermal deposition from a quartz crucible housed in a Knudsen-type effusion cell. Under these growth conditions, the molecules form coherent films with grain sizes of about 100 nm and weak surface roughness comprising a mixture of the bulk α and β phases of PTCDA [1,5,6,14]. All films investigated in this paper were prepared at a stretch starting with a freshly cleaned metal substrate.

The film thickness was determined from the damping of the Ag 3d and Au 4f XPS signals, respectively, by the deposited PTCDA layers. As shown in the inset of Fig. 1, the damping follows a strict exponential Beer-Lambert law with an attenuation length of 3.5 nm at $E_{kin} = 1402$ eV, indicating a predominant layer-by-layer growth of PTCDA for the chosen growth parameters. For analysis of the film structure, a LEED instrument with a microchannel-plate-intensified detector (MCP-LEED) was used, which allows for experiments with extremely low electron currents to avoid electron-beam-induced damage of the molecular films. As an example, Fig. 1 shows the LEED image of 20 ML PTCDA on Au(111), which exhibits the same characteristic diffraction pattern with an apparent sixfold symmetry that is known for 1 ML PTCDA/Au(111) [26], demonstrating the high quality of the so-prepared epitaxial films.

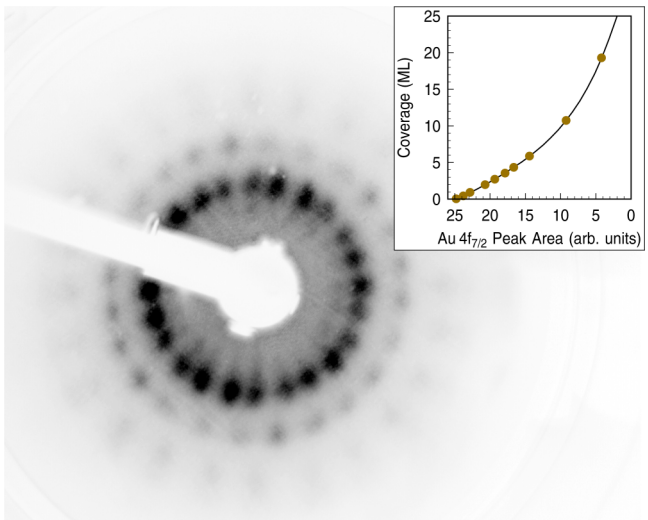

FIG. 1. MCP-LEED image of 20 ML PTCDA on Au(111) with $E = 15$ eV. Inset: Damping of the Au 4f XPS signal with increasing film thickness.

After PTCDA deposition, the sample manipulator of the UHV chamber was cooled down with liquid nitrogen. A constant temperature of 90 K was obtained at the sample surface throughout the PL measurements.

Three different laser systems were used for PL excitation. PL experiments on the silver substrate were conducted either at $\hbar\omega_{exc} = 2.43$ eV with the frequency-doubled pulses from an optical parametric amplifier (OPA) pumped by a 100 kHz Ti:sapphire regenerative amplifier, or with the frequency-doubled pulses of an 80 MHz Ti:sapphire oscillator at $\hbar\omega_{exc} = 3.1$ eV. Both laser systems provided pulses with a temporal width around 50 fs (FWHM). For the experiments on the PTCDA/Au(111) system, an 80 MHz optical parametric oscillator (OPO) was used with an output photon energy of $\hbar\omega_{exc} = 2.37$ eV and 250 fs pulse duration. The PL radiation from the sample was collected with an optical system with a high numerical aperture of 0.45 and was analyzed by means of a spectrograph in Czerny-Turner configuration in combination with a streak camera (Synchrosan FESCA C6860, M6861, Hamamatsu). Data aquisition with the streak camera was triggered with the help of stray light from the excitation laser pulses, which was detected with a fast photodiode. The streak camera was operated either in a slow-streaking mode with a scan range of 2 ns and a time resolution of 15 ps or in a fast-streaking mode with a scan range of 100 ps and a time resolution of 4 ps, which was largely determined by the quality of the trigger signal. Additional time-integrated PL spectra were recorded with an intensified CCD camera (Andor iStar).

III. RESULTS AND DISCUSSION

A. Photoluminescence from PTCDA films

Before we present the results from time-resolved PL experiments, we first discuss the time-integrated PL spectra of PTCDA films and introduce the spectral signatures of excitons in these films. PL spectra of PTCDA films with varying thickness on Ag(111) and on Au(111) are shown in Figs. 2(a) and 2(b), respectively, together with the featureless PL signal from the bare metal surfaces at the bottom of each panel. We start with the discussion of the PL spectra from PTCDA on Ag(111) [Fig. 2(a)]. For a single monolayer (1.0 ML), no PL signal can be detected from the sample. This is a consequence of the fact that the F-LUMO of PTCDA becomes partially filled upon chemisorption on the Ag(111) surface [10], inhibiting optical excitation of the PTCDA molecules in direct contact to the metal. For a coverage of 1.8 ML, two emission bands are observed at 2.10 eV (M) and 1.93 eV (M_{vib}). The PL spectrum closely resembles the solution spectra of PTCDA

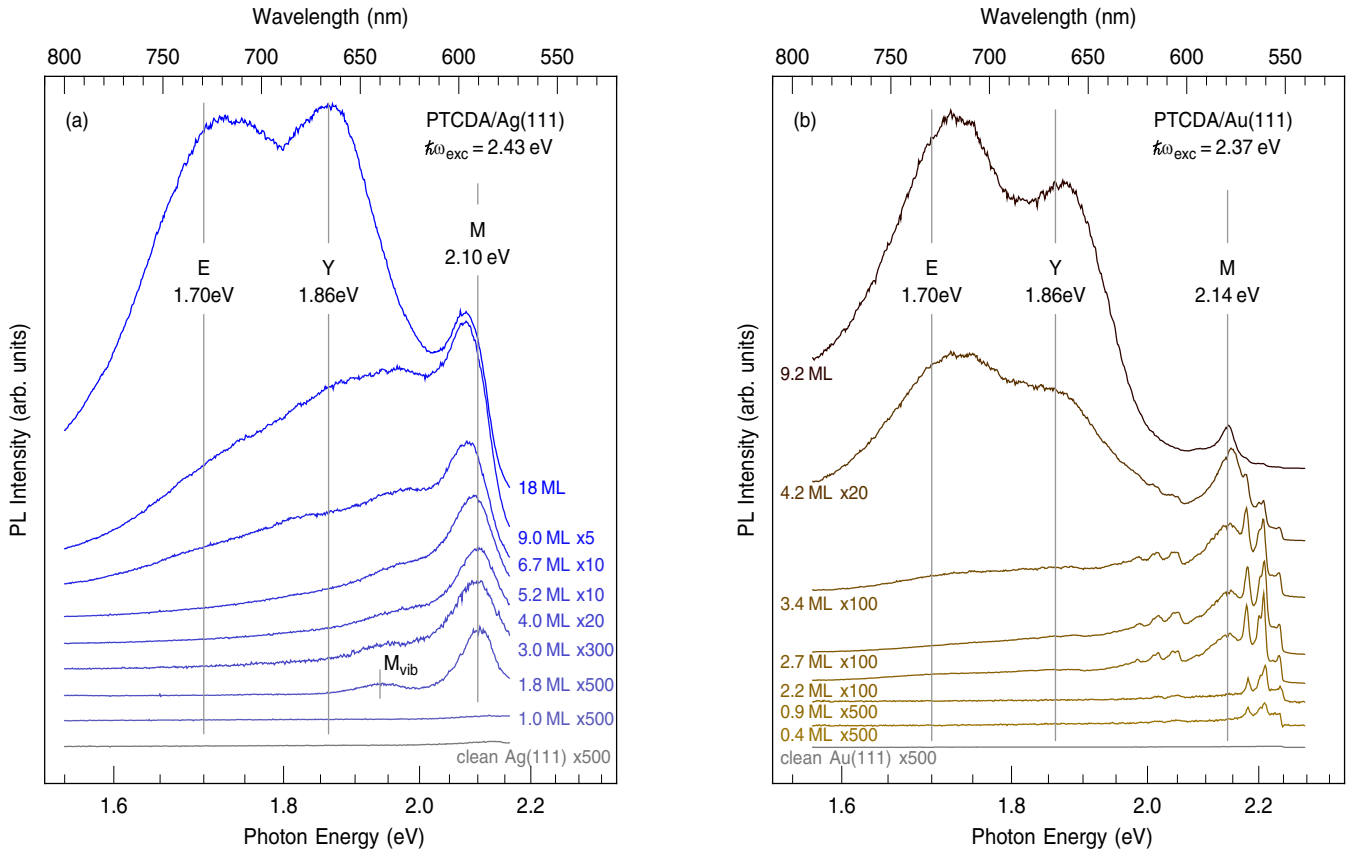

FIG. 2. Time-integrated photoluminescence spectra of PTCDA films (a) on Ag(111) and (b) on Au(111) for increasing film thickness. Vertical lines indicate the spectral positions of the emission bands corresponding to the PTCDA monomer (M), the charge-transfer exciton (Y), and the excimer (E).

dissolved in dimethyl sulfoxide (DMSO) with low concentrations [18], where only PTCDA monomers contribute to the PL signal. On nonconductive substrates where the first PTCDA layer is only physisorbed and optically active, monolayer spectra very similar to the monomer spectrum have been observed before [27]. That means that intralayer coupling has only a little effect on the PL spectrum of PTCDA molecules. For the molecules in the second layer in our experiment, no adjacent molecular layers are available for electronic coupling and, as a consequence, PL from the second-layer molecules reproduces the monomer spectrum of PTCDA in DMSO [18]. Therefore, it is reasonable to assign the M band to emission from vertically decoupled PTCDA molecules. Our assignment is supported by the appearance of the vibronic progression M_{vib} 0.17 eV below M, which is in good agreement with the vibronic shift of 0.15 eV in solution [18] and perfectly agrees with results of PL [27] and differential reflectance spectroscopy (DRS) experiments [28] for submonolayer films on KCl and mica, respectively. In summary, we assign the monomerlike emission bands M and M_{vib} to an excited state of vertically decoupled PTCDA molecules and its vibronic progression. In the following, the term "monomer" will refer to such PTCDA molecules without interlayer coupling, which should not be confused with truly isolated molecules.

Interestingly, the M emission band does not vanish with increasing PTCDA coverage but remains also for thick films, which points to the presence of PTCDA monomers within these films. PL spectral features near 2.1 eV have been reported for thicker PTCDA films above 25 ML PTCDA previously [13,29]. However, because of the more complicated electronic structure of these bulklike PTCDA films, the features could not unambiguously be assigned to specific electronic states of PTCDA but were tentatively attributed to defect-stabilized excitons at interphase boundaries between α- and β-PTCDA. Here, by comparison of PL spectra from PTCDA films with systematically increased thickness, the monomer-related origin of this emission band becomes obvious.

Notwithstanding the persistent monomer contribution M, with increasing film thickness the PL spectrum gradually evolves from the monomer spectrum at 1.8 ML coverage to a bulklike spectrum at 18 ML with distinct emissions bands at 1.7 eV (E) and 1.88 eV (Y) due to excitonic interaction between PTCDA molecules in different layers. Our spectrum at 18 ML closely resembles the spectrum obtained by Wagner *et al.* for a 36 nm PTCDA film on Si(001) at 80 K [19] and is in qualitative agreement with the PL spectrum from 30 ML PTCDA on Ag(111) measured at a lower temperature of 20 K by Schneider *et al.* [13]. We observed very similar bulklike spectra also for thinner films after annealing the sample at temperatures around 400 K (not shown), which is known to facilitate the formation of three-dimensional PTCDA

clusters [30]. The E and Y lines in Fig. 2 are placed at the corresponding transition energies observed for these PTCDA crystallites. Most authors assign the low-energy feature E to self-trapped CT excitons or excimers, based on its long radiative lifetime and its spectral blueshift with increasing temperature [4,13,21,23,24]. For thicker films of PTCDA, the intensity of the E band was found to strongly depend on the growth conditions, i.e., the film morphology [4,13]. The strongest relative intensity of the E emission was found for growth temperatures that facilitate a coexistence of the α and β phases of crystalline PTCDA, indicating that the formation of excimers is supported by stacking faults between the α- and β-configurations of PTCDA in this intermediate structure [13]. The comparatively strong intensity of the E band in our spectra from thicker films in Fig. 2 is consistent with a film growth in the intermediate structure at 273 K [13]. The Y band at 1.88 eV has been assigned to excitons with mixed Frenkel and CT character which, because of the negative dispersion of the exciton band, recombine with a significant Stokes shift at the Brillouin zone boundary [13,16]. An additional emission band at 1.95 eV, which has been observed at lower sample temperatures by other groups [13,19,21] and corresponds to nonrelaxed excitons [21], is absent in our PL spectra. This is in agreement with Ref. [19], where a strong quenching of this state is observed for temperatures of 80 K and above.

On the Au(111) substrate, Raman bands of PTCDA are readily observed around 2.2 eV even for submonolayer coverages [Fig. 2(b)]. The observed Raman shift of 0.17 eV (1371 cm^{-1}) of the most intense band agrees well with Raman spectra of PTCDA on gold [31] and, moreover, is consistent with the vibronic shift of the monomer peak M_{vib} in Fig. 2(a). The high intensity of the observed Raman signal can be explained by surface enhancement due to the coupling with surface plasmon polaritons (SPPs) at a nearby energy of 2.5 eV [32]. In contrast, on the silver substrate no Raman signal can be observed, which is in agreement with the SPP of silver at a significantly higher energy of 3.5 eV, well above the excitation energy of 2.43 eV in our experiment. Above 1 ML coverage, the monomer-related emission band M evolves, partially obscured by the increased Raman signal at virtually the same spectral position. Its vibronic progression M_{vib} is likewise superposed by PTCDA Raman bands, and therefore cannot be resolved in Fig. 2(b). With further increasing film thickness, we essentially observe the same transition from the monomer spectrum at lower coverages to the bulklike spectrum for thicker PTCDA films as in the case of the Ag(111) substrate. However, on Au(111) this transition has already far progressed at a much smaller film thickness of only 4 ML. A monomer-to-bulk transition with increasing film thickness has also been reported for the optical absorption of PTCDA on mica by Proehl *et al.* [28,33]. On this nonconductive substrate, the transition is virtually completed upon deposition of two layers of PTCDA. This agrees with time-integrated PL data for PTCDA/KCl by Schlettwein *et al.* [34], who demonstrate a striking change of the PL spectrum progressing from 1 ML to 2 ML PTCDA. In contrast, on Au(111) a film thickness of at least two to four PTCDA layers is needed for the transition to a bulklike spectrum [28]. Exactly the same effect is observed in our PL experiment where the bulklike exciton-related emission bands E and Y evolve at coverages between 3 ML and 4 ML PTCDA and are suppressed for thinner films on Au(111) [Fig. 2(b)]. This metal-induced quenching effect

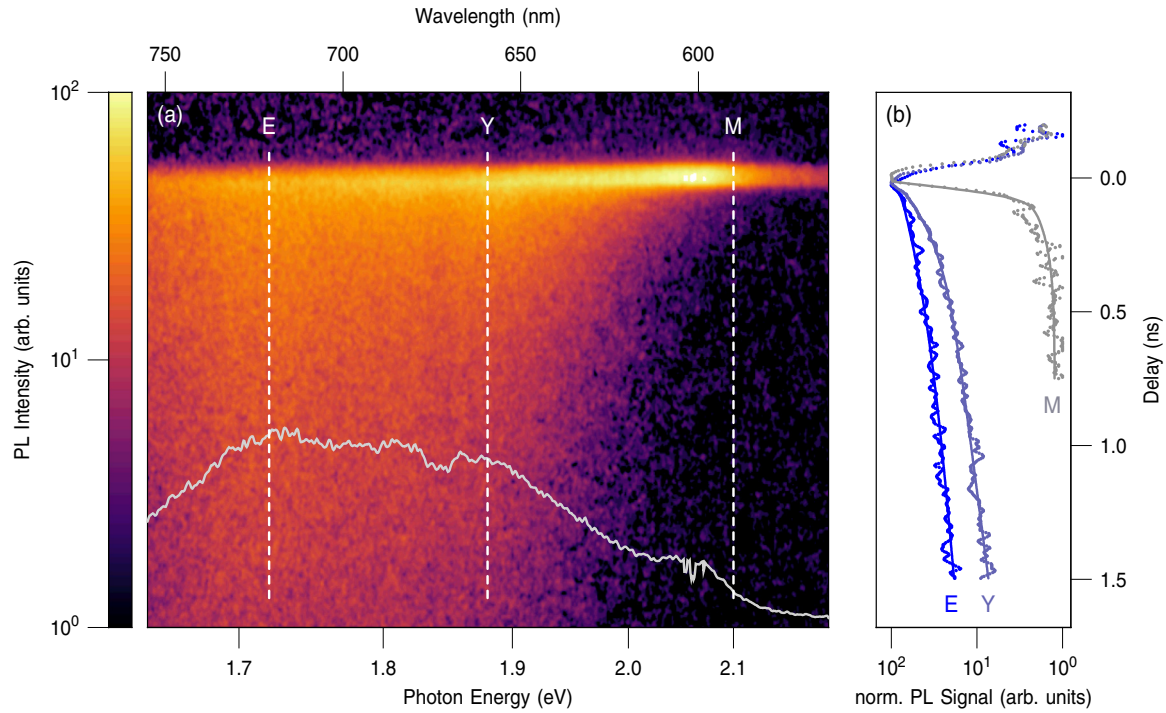

FIG. 3. (a) False-color presentation of the time- and photon-energy-resolved photoluminescence of 14 ML PTCDA on Ag(111) with the time-integrated spectrum as gray curve. The PL data was obtained with $\hbar\omega_{exc} = 3.1$ eV. (b) PL transients along the dashed lines in (a) normalized to maximum intensity. The solid lines represent triexponential fits.

is even more pronounced on Ag(111), where more than 9 ML are needed for a bulklike PL spectral shape [Fig. 2(a)]. As we will show in the following, the suppression of PL from these bands can be related to efficient nonradiative relaxation of excitons due to interaction with the conduction electrons of the metal substrates.

We now turn to the results of time-resolved PL experiments, which reveal that the relaxation dynamics of the different excitonic states in PTCDA films take place on different timescales. In Fig. 3, we present PL data of 14 ML PTCDA on Ag(111) obtained with the streak camera in slow-streaking mode. In Fig. 3(a), the time- and photon-energy-resolved PL signal is plotted on a logarithmic false-color scale. The gray curve represents the time-integrated spectrum on a linear scale which again exhibits the three emission bands E, Y, and M. From the corresponding transient PL signals in Fig. 3(b), it follows that the monomer excitation M decays within a few picoseconds. The excitonic states E and Y are much longer lived and, as a consequence, the corresponding bands can be observed in Fig. 3(a) on a nanosecond scale. Note, however, that the exciton lifetimes in the metal-supported PTCDA films of our experiments are considerably shorter than the lifetimes between 13 ns and 53 ns reported for α-PTCDA bulk crystals [24] (cf. also Fig. 4). Obviously, additional nonradiative relaxation channels are provided by the metal substrate, which agrees with our findings from time-integrated PL (Fig. 2). Interaction with the metal substrate should be an important relaxation pathway for excitons in the thin molecular films of our experiment. For this reason, the exciton lifetime within a PTCDA layer should strongly depend on its distance to the metal surface. With photon energies well below the onset of the optical absorption of PTCDA around 2.2 eV, reabsorption of the PL radiation is negligible in our experiment. Therefore, all PTCDA layers, except the first one, equally contribute to the overall PL signal, each of them with a particular decay rate depending on the respective molecule–metal separation.

To assess the influence of the film thickness on the exciton dynamics, the transient signals were measured for PTCDA films on Ag(111) and on Au(111) with systematically varying film thicknesses. For each film thickness, we use the time constants of a triexponential fit as a first estimate of the excitonic lifetimes of E, Y, and M, thereby averaging over the different lifetimes within the different molecular layers. A more detailed analysis which also accounts for the contributions of the individual layers will be given in the following Secs. III B and III C. In Fig. 4, the lifetimes derived in this manner are plotted as a function of the film thickness. The lifetimes obtained for the monomer-related state M are of the order of few picoseconds, probably shorter than the time resolution of about 4 ps in our experiment, and do not significantly depend on the number of PTCDA layers. In contrast, the lifetimes of the excitonic states E and Y strongly decrease with decreasing film thickness, reflecting the stronger coupling to the metal of the PTCDA layers closer to the substrate. Interestingly, as a function of film thickness, the lifetimes decrease much stronger on the silver substrate than on gold, indicating much more efficient exciton–metal coupling for this substrate.

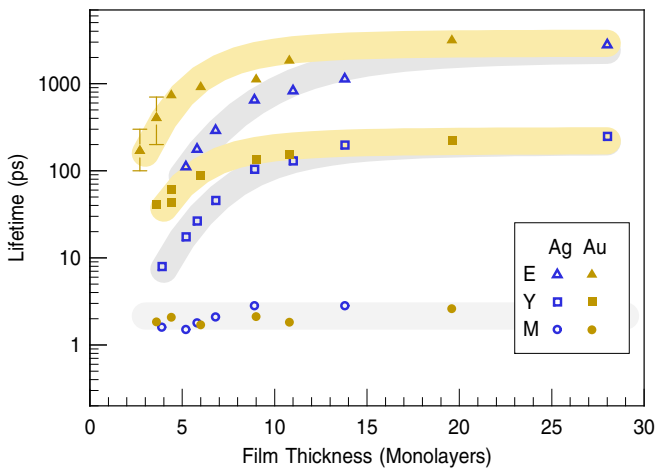

FIG. 4. Lifetimes of the excitonic states E, Y, and M as a function of the PTCDA film thickness obtained with time-resolved photoluminescence.

B. Relaxation dynamics of state E

To gain more insight into the relaxation mechanisms that govern the metal-induced exciton quenching, we compare the transient PL signals for the different PTCDA films with model calculations. First, we focus on the decay of the low-energy emission band E. As this state presumably originates from excimers at stacking faults between molecules of adjacent PTCDA layers, the corresponding excitons should be immobile, especially along the stacking direction perpendicular to the sample surface. Accordingly, we model the E excitons as point dipoles which are localized at a specific distance d from a plane metal surface and which relax due to dipole interaction with the conduction electrons of the metal. Quenching of fluorescence from molecules in front of a metal surface was first treated within the so-called CPS theory by Chance, Prock, and Silbey [35] in which the molecule is regarded as an oscillating dipole interacting with its image dipole in the metal. Essentially, bulk loss-processes in the metal are responsible for energy dissipation in CPS theory, which reasonably describes energy transfer at larger dipole–metal separations d with a d^{-3} dependence of the loss rate. For shorter distances, surface-specific dissipation channels like electron–hole-pair excitation in the metal surface region become important and can be theoretically described by a modification of CPS theory [36]. This is often referred to as surface-damping theory and leads to a d^{-4} dependence of the loss rate. Here, we adopt a more general surface-damping approach formulated by Ford and Weber [37]. As it is largely related to surface-damping theory, we name it the surface-damping model in the following.

In the surface-damping model, the fluorescence of a molecule near a metal surface is described as an oscillating point dipole $\boldsymbol{\mu} \cdot e^{i\omega t}$ in a dielectric medium ϵ_1 above a semi-infinite metal. Briefly, the electric field of the point dipole is expanded into plane waves and the dissipated power,

$$P = \frac{\omega}{2} \mathrm{Im}[\boldsymbol{\mu}^* \cdot \mathbf{E}], \tag{1}$$

in the resulting electric field $\mathbf{E}$, including the field reflected from the metal surface, is calculated as a function of the surface wave vector $\mathbf{k}_\parallel$. The thickness of the molecular films in

our experiment is below 10 nm, i.e., significantly smaller than the wavelength of the emitted radiation, which allows us to work within quasistatic approximation. The transition dipole moment for CT excitons in PTCDA crystals approximately lies parallel to the molecular planes [16]. We therefore assume an electric dipole moment $\boldsymbol{\mu}$ parallel to the metal surface, which in quasistatic approximation yields

$$P = \frac{\omega}{2\epsilon_1}\,\mathrm{Re}\left[\frac{\mu^2}{2}\int_0^\infty \mathrm{d}k_\parallel\,\frac{k_\parallel}{k_\perp}\left(k_1^2 + k_\perp^2\left(1 - r_{12}^{\mathrm{P}}\,e^{2ik_\perp d}\right)\right)\right], \quad (2)$$

where $k_1^2 = \epsilon_1 \frac{\omega^2}{c^2}$ is the squared wave vector in medium ϵ_1 and $k_\perp = \sqrt{k_1^2 - k_\parallel^2}$ its normal component [37]. As only the absolute value $\mu = \sqrt{\boldsymbol{\mu}\cdot\boldsymbol{\mu}^*}$ enters Eq. (2), we will call μ the electric dipole moment in the following. r_{12}^{P} is the reflection coefficient for the p-polarized component of the electric field at the metal surface. If the metal is described by a local dielectric function $\epsilon_2(\omega)$, the reflection coefficient is simply given by the Fresnel formula:

$$r_{12}^{\mathrm{P}}(\omega) = \frac{\epsilon_2(\omega) - \epsilon_1}{\epsilon_2(\omega) + \epsilon_1}\,. \quad (3)$$

Within this local approximation, transfer of momentum from the dipole field to conduction electrons of the metal is not explicitly considered. However, for small molecule-metal separations, a significant amount of momentum can be provided by the dipole near field, giving rise to electron–hole excitations inside the metal. Such nonlocal effects can be accounted for with a generalized form of the reflection coefficient,

$$r_{12}^{\mathrm{P}}(k_\parallel, \omega) = \frac{1 - \epsilon_1 \frac{k_\parallel}{\pi}\int_0^\infty \frac{\mathrm{d}q}{k^2\epsilon_l(k,\omega)}}{1 + \epsilon_1 \frac{k_\parallel}{\pi}\int_0^\infty \frac{\mathrm{d}q}{k^2\epsilon_l(k,\omega)}}\,, \quad (4)$$

where $k^2 = k_\parallel^2 + q^2$ is the squared wave vector inside the metal and $\epsilon_l(k,\omega)$ is the longitudinal k-dependent (Lindhard) dielectric function [37].

Figure 5 displays how the dissipated power of a point dipole, oscillating at $\hbar\omega = 1.7$ eV in front of a silver surface, changes with its distance to the metal. For the local model (red dots), the dielectric function was directly calculated from tabulated data of the optical constants of silver [38]. For the nonlocal model (blue dots), additional Drude parameters are needed to calculate the dielectric function $\epsilon_l(k,\omega)$ (cf. Eqs. (2.30)–(2.33) in Ref. [37]). We obtain the Drude parameters, i.e., the plasma frequency $\hbar\omega_{\mathrm{P}} = 9.21$ eV, the Drude scattering rate $\hbar\nu = 0.0255$ eV, and the background dielectric constant $\epsilon_{\mathrm{b}} = 3.903$ from a fit of $\epsilon_l(0,\omega)$ to the local dielectric function with a fixed Fermi velocity of $v_{\mathrm{F}} = 1.4 \times 10^8$ cm s^{-1} [39]. Both the local and the nonlocal model use an effective dielectric constant $\epsilon_1 = 3.7$ of PTCDA [16]. At larger distances above 100 Å, the dissipated power P, which is proportional to the relaxation rate $\Gamma = P/\hbar\omega$, is basically the same in both models and does not strongly vary with the dipole–metal separation. At these large distances, relaxation of molecular excitations is dominated by radiation of photons and coupling to SPPs of the metal. Only electric field components with a small parallel momentum, not much larger than the SPP wave

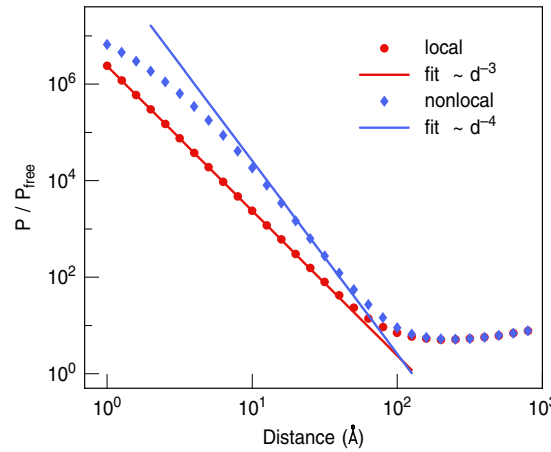

FIG. 5. Power loss of an oscillating electric dipole with $\hbar\omega = 1.7$ eV in front of a silver surface as a function of its distance to the metal. The dissipated power is normalized to the power P_{free} radiated by a free dipole in vacuum. A local (red) and a nonlocal (blue) model was used for the dielectric function of silver. Dashed lines represent approximations of the full calculations with a pure d^{-3} and d^{-4} dependence, respectively.

vector k_{SPP}, contribute to these processes [37]:

$$k_\parallel \lesssim k_{\mathrm{SPP}} = \frac{\omega}{c}\sqrt{\frac{\epsilon_1\,\epsilon_2}{\epsilon_1 + \epsilon_2}}\,. \quad (5)$$

At shorter distances, the larger $k_\parallel$ components also become important. In that case, the evanescent waves of the oscillating dipole can couple to the conduction electrons of the metal giving rise to energy losses due to scattering as described by the imaginary part of the dielectric function. For this reason, the shape of the dissipation curves in Fig. 5 strongly depends on the underlying model for the metal response. In the local model (red dots) where energy dissipation is mainly due to electron–electron interaction, the relaxation rate follows a d^{-3} law (red line), d being the dipole–metal separation. If the metal is described by a nonlocal dielectric function (blue diamonds) the calculated relaxation rate exhibits a much stronger rise with decreasing distance and, in the case of silver, can be well described by a d^{-4} law (blue line) for medium distances between roughly 5 Å and 50 Å. The much higher energy transfer to the metal can be explained by an additional dissipation channel constituted by electron–hole excitations, i.e., intraband transitions of the conduction electrons which are accompanied by transfer of parallel momentum up to a maximum value of

$$k_{\parallel,\max} = \sqrt{2m_{\mathrm{e}}\omega/\hbar + k_{\mathrm{F}}^2} + k_{\mathrm{F}}\,. \quad (6)$$

Because of this cutoff wave vector for electron–hole excitations and an additional screening of electron–electron scattering for large wave vectors, which is not accounted for in a local approximation, the dissipation curve flattens again for very short dipole–metal separations in the nonlocal model. From an analogous treatment of a gold substrate (not shown), it follows that in the range of distances relevant for the molecular films in our experiment, the local and the nonlocal calculations diverge much less, so that the distance-dependent relaxation rate is well-described by a local d^{-3} law. This

TABLE I. Distances between adjacent PTCDA layers used for the model calculations in Figs. 6 and 7.

	Ag(111)	Au(111)
s (Å)	3.24	
s_{01} (Å)	2.86	3.27
s_{12} (Å)	3.10	3.24

means that in the case of gold as a substrate, electron–electron scattering is the dominant dissipation channel and nonlocal effects such as intraband transitions play a minor role for surface damping of molecular excitations. We now compare the experimental PL transients to calculated transients within the model presented above. As already argued earlier, each PTCDA layer except the first one equally contributes to the full transient with an individual lifetime depending on its distance to the metal substrate. We assume a distance $s = 3.24$ Å between two adjacent PTCDA layers, which is the average layer separation of the α and β phases of crystalline PTCDA [40] (all geometric parameters are summarized in Table I). In the case of Ag(111), we further take into account the binding distance of $s_{01} = 2.86$ Å between PTCDA and the Ag(111) surface [9], and a separation $s_{12} = 3.1$ Å between the first and the second molecular layer. The latter value, which is the average of the PTCDA–Ag(111) binding distance and the molecular layer separation in β-PTCDA, was chosen because of the structural similarity of the second PTCDA layer with the crystalline β phase [8]. For the Au(111) substrate, a larger binding distance $s_{01} = 3.27$ Å was used for the first molecular layer, which essentially is the sum of the van der Waals radii of Au and C atoms reflecting the relatively week physisorption of PTCDA on gold [41]. For the separation of the first and the second molecular layers on Au(111), the same value as for all other layers was used, i.e., $s_{12} = s = 3.24$ Å. While the results of our model calculation for the state E do not crucially depend on the exact values of the molecule–metal distances for the first two layers, these distances will be important parameters for a correct description of the CT exciton related state Y presented later in this paper. The strength of the transition dipole μ is not *a priori* known and remains the only adjustable parameter to match the model transients to the experimental data.

First, we investigate the quenching of the E state on the silver substrate. Figure 6(a) compares the experimental transient PL recorded at the spectral position of the E emission band (thin lines) with calculated transients from the (nonlocal) surface-damping model (thick solid lines). For the latter, each molecular layer was assumed to contribute equally to the overall signal with its particular distance-dependent decay rate,

$$\Gamma_{\text{dipole}}(d) = \frac{1}{\tau(d)} = \frac{P(d)}{\hbar\omega}, \tag{7}$$

where $P(d)$ is the distance-dependent energy-loss rate obtained from a full nonlocal calculation according to Eqs. (2) and (4). All transients are normalized to a maximum value of one at zero time delay. With a transition dipole moment of $\mu = 2.96$ Debye, the surface damping model well reproduces

TABLE II. Summary of the decay and transfer rates used for the model calculations in Figs. 6 and 7.

	Ag(111)	Au(111)
Γ_{rad} (ps^{-1})	4.67×10^{-5}	
E:		
$b_{\text{dipole,Ag}}$ (Å^{4}ps^{-1})	1000	
$b_{\text{dipole,Au}}$ (Å^{3}ps^{-1})		4.0
Y:		
Γ_{hop} (ps^{-1})	0.4	
$\Gamma_{2\to1}$ (ps^{-1})	3.0	0.17
$\Gamma_{1\to0}$ (ps^{-1})	17.0	2.0

the experimental data. The dashed lines in Fig. 6(a) represent a simplified model where the exciton lifetime in each layer scales with the fourth power of its distance d to the metal surface. As expected (cf. Fig. 5), the full model also nicely agrees with this simplified model based on a d^{-4} law,

$$\Gamma_{\text{dipole,Ag}} = b_{\text{Ag}} \cdot d^{-4}, \tag{8}$$

with $b_{\text{Ag}} = 1$ Å^4 fs^{-1} (all decay rates and transfer times are summarized in Table II). Note that the surface-damping model inherently includes radiative losses, as it directly follows from Poynting's theorem formulated for a point dipole in Eq. (1). The simplified model in Eq. (8) approximates the full calculation for dipol–metal distances below 10 nm where radiative losses are orders of magnitude smaller than the metal-related dissipation channels (cf. Fig. 5), i.e., radiative losses are neglected in Eq. (8).

Remarkably, only a single adjustable parameter, the dipole strength μ, is necessary to simultaneously reproduce the full shape of the experimental transients for all PTCDA film thicknesses. Its value of 2.96 Debye appears reasonable in comparison to the $S_0 \to S_1$ transition dipole moment of the free molecule $\mu_{\text{free}} = 7.4$ Debye and values between 1 Debye and 2 Debye for the optical excitation of CT excitons obtained from analysis of optical absorption spectra [16]. Only for thicker films and at short temporal delays, the model calculations deviate from the experimental results. Presumably, the additional contribution at smaller delays to the experimental signal stems from the partial spectral overlap with the shorter-lived Y emission, which cannot be completely spectrally separated from the E emission band in our experiment (cf. Figs. 2 and 3). In conclusion, the good agreement of our model with the experimental data clearly supports our interpretation of the low-energy spectral feature E as an immobile excimer or self-trapped CT state that relaxes due to dipole interaction with electrons in the silver substrate.

In Fig. 6(b), we apply the same analysis of the E state relaxation to PTCDA films deposited on Au(111). In the case of gold, however, the agreement of our calculations with the experimental transients is by far not as good as for the films deposited on silver. Especially for thicker films, we observe strong contributions with rather short lifetimes to the overall shape of the experimental transients. We achieve much better agreement if we renormalize the theoretical curves to match the experimental transients at larger temporal delays, thereby neglecting the shorter-lived contributions. Presumably, the

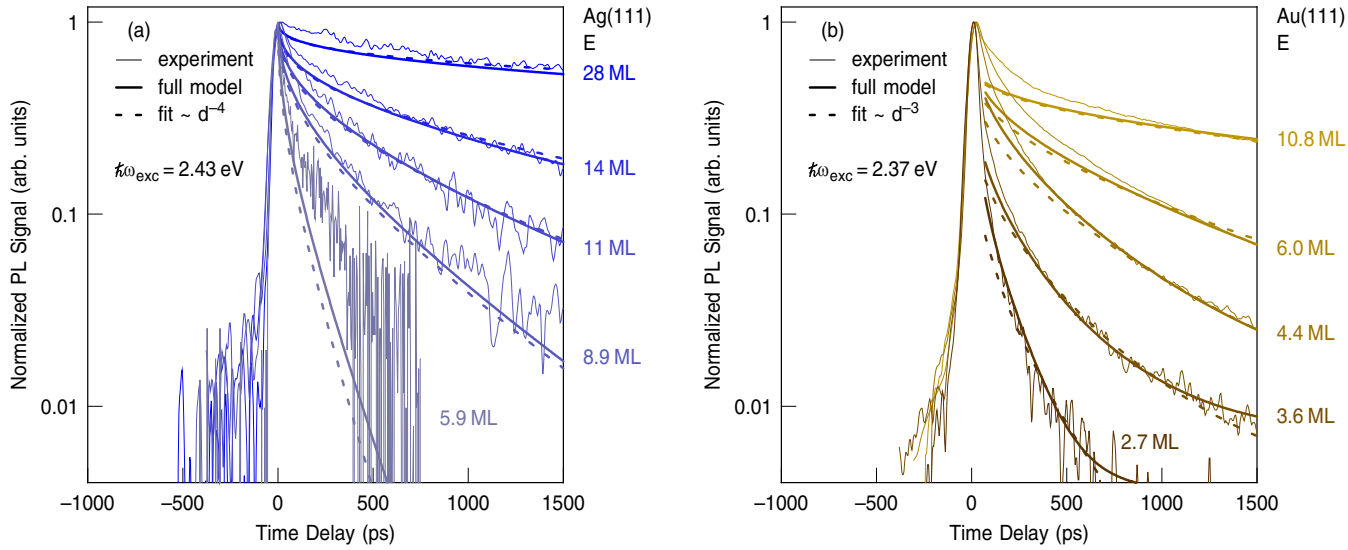

FIG. 6. Normalized transient photoluminescence from state E for PTCDA films of different thicknesses (a) on Ag(111) and (b) on Au(111). Thick solid lines are scaled results from surface damping theory, dashed lines correspond to a model with (a) a d^{-4} dependence and (b) a d^{-3} dependence of the relaxation rate on the distance d to the metal surface.

deviation of the modeled transients from the experimental ones at smaller delays again stems from the spectrally overlapping Y emission, which, because of its larger lifetime on Au(111), has a stronger influence on the shape of the transients than for the PTCDA/Ag(111) system. Also, a small additional long-lived contribution to the overall PL is observed, especially for thinner films below 5 ML. Better agreement of the experimental data with the renormalized theoretical curves is achieved if we refine our model by addition of a small PL background with a distance-independent lifetime of 21.4 ns. This is the PL lifetime observed in another experiment for large PTCDA crystallites (cf. Sec. III A). A very similar radiative lifetime of 25 ns has been observed before for the excimer state in bulk α-PTCDA [24]. Probably, due to the weak binding of PTCDA molecules to the gold surface compared to silver, PTCDA tends to form clusters more easily on Au(111) leading to the presence of some PTCDA crystallites responsible for the weak long-lived PL signal in Fig. 6(b) already for films below 5 ML. Nevertheless, also on Au(111), the decay of the E luminescence can be explained by energy transfer from vertically localized excitons to the metal via dipole interaction. Note that, again, a simplified model [dashed lines in Fig. 6(b)], now based on a d^{-3} law for the relaxation rate, yields similar results as the full calculation (solid lines). As for the full calculation, also for the simplified model, an additive distance-independent PL background to the transient intensity $I(t)$ is considered according to

$$I(t) = (1 - f) \cdot e^{-\Gamma_{\mathrm{dipole,Au}} \cdot t} + f \cdot e^{-\Gamma_{\mathrm{rad}} \cdot t}, \tag{9}$$

where $\Gamma_{\mathrm{rad}} = \tau_{\mathrm{rad}}^{-1} = (21.4\,\mathrm{ns})^{-1}$ is the distance-independent radiative decay rate of bulk PTCDA and f is the fraction of the bulklike background to the overall PL signal which is below 0.015 for all of the curves in Fig. 6(b). For the distance-dependent main contribution, the simplified model yields

$$\Gamma_{\mathrm{dipole,Au}} = b_{\mathrm{Au}} \cdot d^{-3}, \tag{10}$$

with $b_{\mathrm{Au}} = 0.004$ Å^3 fs^{-1}. The apparent cubic relation between the lifetime and the molecule–metal distance reflects that interband transitions play a minor role for energy dissipation at the gold surface, in contrast to our results for the silver substrate.

C. Relaxation dynamics of state Y

After discussion of the E luminescence, we now turn to the Y emission band. In Fig. 4, we saw that on both substrates the Y emission decays roughly one order of magnitude faster than the PL from state E. Like the E luminescence, also the lifetime of state Y dramatically decreases with the PTCDA film thickness and, again, this decrease is much stronger on the silver substrate than on gold. While thick films exhibit comparable lifetimes on both subtrates, for thin films the Y lifetime on silver eventually becomes roughly one order of magnitude smaller than on gold.

Figure 7 displays the experimental PL transients recorded at the spectral position of the Y emission band with high time resolution for delays below 70 ps. As before, we try to model the shape of the transient PL signals in Fig. 7 as superpositions of the luminescence from several PTCDA molecular layers, each of them with an individual decay rate depending on its distance to the metal substrate. In contrast to the E emission, no satisfactory agreement with the experiment could be found for models with a d^{-3} or a d^{-4} decrease of the relaxation rate or with the full surface-damping model alone. Accordingly, surface damping seems to play a minor role for the decay of the Y luminescence. Another relaxation pathway, which has not been considered so far, involves the diffusion of excitons. As mentioned earlier, the excitons corresponding to state Y are argued to have a strong CT character [16,21]. They should generally be mobile, at least along the stacking direction where the electronic coupling of adjacent PTCDA molecules is rather strong. After diffusion to the PTCDA/metal interface, the CT excitons can be annihilated by the creation of

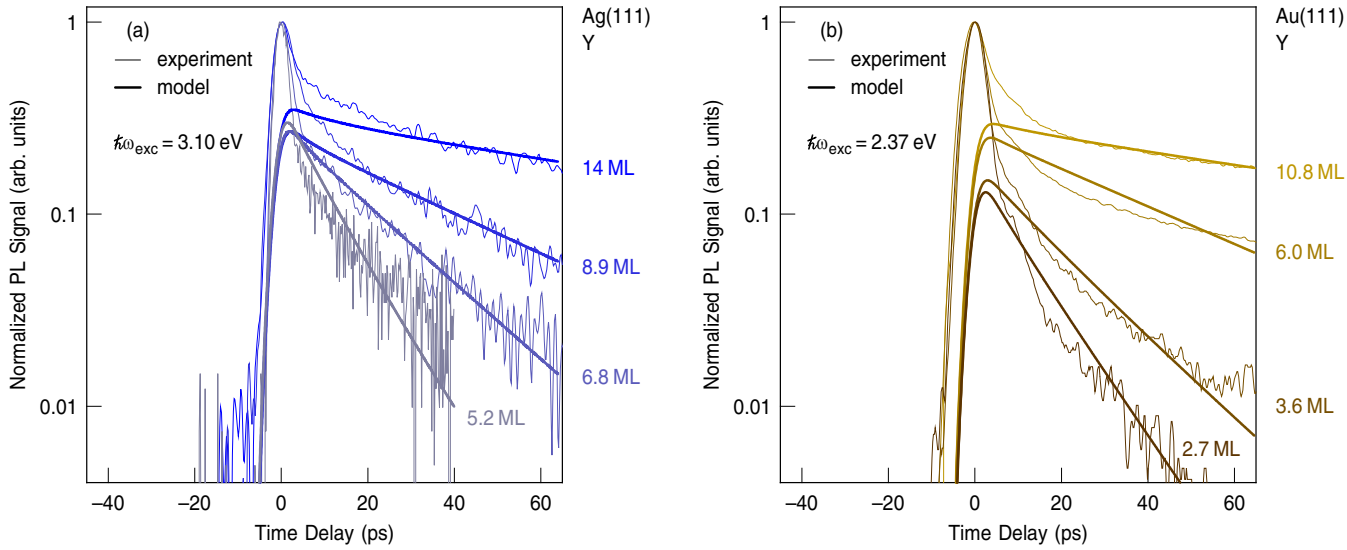

FIG. 7. Normalized transient photoluminescence from state Y for PTCDA films of different thicknesses (a) on Ag(111) and (b) on Au(111). Thick solid lines are results from a model based on exciton diffusion along the stacking direction with the transfer rates given in Table II.

hot electrons inside the metal. In fact, earlier results by other groups from PL experiments on PTCDA/TiOPc heterostructures [42] as well as from transient-absorption experiments on thicker PTCDA films [43] could be explained assuming one-dimensional diffusion of excitons through the molecular films.

To account for the diffusion of CT excitons through the PTCDA films, we employ a hopping model, which describes the diffusion of excitons by hopping between adjacent molecular layers with a hopping rate Γ_{hop}. Exciton depopulation by surface damping is considered as well as described in the preceding Sec. III B for state E. For simplicity, we do not apply the full surface-damping model but use the simplified Eqs. (8) and (10) with a d_i^{-4} and d_i^{-3} dependence on silver and on gold, respectively, where d_i is the molecule–metal separation of the ith PTCDA layer. As the simplified models do not account for radiative decay, we explicitly introduce a decay rate $\Gamma_{rad} = 4.67 \times 10^{-5}$ ps^{-1} = (21.4 ns)$^{-1}$. Note that here Γ_{rad} describes an additional radiative decay channel, in contrast to Eq. (9) where it entered as an independent signal contribution to account for possible PTCDA clusters on the sample surface. The change of the exciton population dn_i/dt within a layer i is then given by

$$\frac{dn_i}{dt} = \Gamma_{pump} + (n_{i+1} + n_{i-1} - 2n_i)\Gamma_{hop} - \Gamma_{i,dipole} - \Gamma_{rad} . \quad (11)$$

Γ_{pump} describes the initial pumping of the exciton population by the laser pulse which is assumed to be homogeneous throughout the PTCDA film. $\Gamma_{i,dipole}$ is the surface damping rate in the ith layer according to Eqs. (8) and (10). As approximate values, we use the parameters $b_{Ag} = 1$ Å^4 fs^{-1} and $b_{Au} = 0.004$ Å^4 fs^{-1} obtained from the analysis of the E emission presented in the preceding section. The second term in Eq. (11) describes how the exciton population in the ith layer changes due to hopping of electrons from the adjacent layers $i+1$ and $i-1$ into i and vice versa. Hopping from the metal back into the first molecular layer is prohibited within this model as well as a loss of excitons out of the outermost layer into the vacuum. To simulate the transient PL from the CT excitons, the system of differential Eq. (11) is numerically solved for 1 fs time steps, then for each time step the exciton population is summed up over all layers, and finally the time-dependent overall population is convolved with a Gaussian of 4.2 ps FWHM to account for the limited time resolution of our experiment (cf. Sec. II).

In Fig. 7, we compare the results of our simulations with the experimental transients obtained from state Y. A strong short-lived contribution to the experimental transients with a lifetime of a few picoseconds is readily recognized for both substrates. As the Y emission overlaps with the M_{vib} emission band and also partially with the M band (cf. Fig. 2), we attribute some short-lived PL intensity in Fig. 7 to luminescence from electronically decoupled PTCDA monomers which might appear at defects in the layered PTCDA film. Also, recombination of CT excitons at grain boundaries within the film might be a reasonable explanation for the PL contributions with short lifetimes. Since such defect-related effects are not included in our model calculations, we again scale the simulated transients (thick lines) to match the experimental data at larger delays, thereby neglecting the short-lived contributions at small delays. The free parameter Γ_{hop} is chosen to reproduce the experimental data at larger delays simultaneously for all film thicknesses and on both substrates. With a value of 0.4 ps^{-1} for Γ_{hop} the longer-lived parts of the transients are well-reproduced for the thicker films above 8 ML. To achieve good agreement also for thinner films, it is necessary to consider the different electronic structure of the first layer of PTCDA molecules in direct contact to the metal surface. Therefore, we introduce different hopping rates $\Gamma_{2\to1}$ between the second and the first organic layer and $\Gamma_{1\to0}$

between the first layer and the metal. The former accounts for a different electronic coupling between the first two molecular layers which is caused by the altered binding distance and the different electronic properties of the first layer, in particular the F-LUMO of PTCDA on Ag(111). The latter describes the transfer of excitons through the first molecular layer, i.e., annihilation of excitons at the molecule/metal interface. These additional transfer rates substantially originate from the molecule–metal interaction, and thus they are not only expected to deviate from the intermolecular hopping rate Γ_{hop} of the layers $i \geqslant 2$ but also to depend on the specific metal substrate.

While, for thick films, the parameters $\Gamma_{2\to1}$, and $\Gamma_{1\to0}$ are adjustable within a rather broad margin without significantly improving or deteriorating the agreement between model and experiment, for thin films they have a strong influence on the shapes of the model curves and on the overall luminescent lifetimes. Good agreement is achieved with the set of transfer rates summarized in Table II. We have to point out that especially for thin films, the PL from the Y state is rather weak and heavily superimposed by the short-lived monomer contributions. Therefore, the values given in Table II must not be understood as definite values but are intended to adumbrate the relative efficiencies of the involved transfer processes. Note that on both substrates the transfer rates exceed the radiative decay rate $\Gamma_{\mathrm{rad}} = 4.67 \times 10^{-5}\ \mathrm{ps}^{-1}$ by several orders of magnitude. Also, decay due to surface damping becomes noticeable only for very thin molecular films. Thus, the main contribution to the decay of the Y emission stems from exciton diffusion and annihilation at the organic/metal interface. The rather large uncertainty of the absolute values in Table II notwithstanding, we conclude that $\Gamma_{2\to1}$ and $\Gamma_{1\to0}$ are approximately one order of magnitude higher on the silver substrate than on gold, which indicates another efficient channel for energy transfer from CT excitons to the metal for this substrate.

In summary, we explain the decay of the Y emission in PTCDA films with a combined model based on surface-damping theory and on the diffusion of CT excitons along the stacking direction of PTCDA with subsequent annihilation at the PTCDA/metal interface. The relaxation dynamics for thick PTCDA films is mainly determined by the mobility of the CT excitons, represented by Γ_{hop}. As expected, Γ_{hop} is a bulk property of the layered PTCDA films and does not depend on the specific metal substrate. Its value of $0.4\ \mathrm{ps}^{-1}$ corresponds to a diffusion constant $D = 4.2 \times 10^{-4}\ \mathrm{cm}^2\ \mathrm{s}^{-1}$, which reasonably agrees with published values of $2 \times 10^{-3}\ \mathrm{cm}^2\ \mathrm{s}^{-1}$ and $5 \times 10^{-3}\ \mathrm{cm}^2\ \mathrm{s}^{-1}$ obtained at temperatures of 90 K and 5 K, respectively [42,43]. For thin films, the relaxation rate is governed by the efficiency of transport through the first molecular layers and annihilation at the PTCDA/metal interface, as described by the transfer rates $\Gamma_{2\to1}$ and $\Gamma_{1\to0}$, which deviate about one order of magnitude for the two metals. The much higher rates on Ag(111) than on Au(111) clearly reflect the stronger binding of PTCDA molecules to the metal which are chemisorbed at the Ag(111) surface, in contrast to the physisorbed molecules on Au(111). A more efficient relaxation process for the first two layers of PTCDA on Ag(111) has been proposed by Gebauer *et al.* before, based on results from time-integrated PL [20]. The authors also address the role of exciton diffusion. However, as they discuss the energy-integrated signal and not the individual emission from state Y, we cannot quantitatively compare their results with ours. Gebauer *et al.* propose hybridized molecule-substrate orbitals responsible for enhanced charge transfer across the interface. Especially in light of the unoccupied metal–organic interface state at the PTCDA/Ag(111) interface, which is well-established in the meantime and which is absent at the PTCDA/Au(111) interface [11,15], this explanation is reasonable. Moreover, the recent work of our group suggests that this interface state constitutes an efficient channel for charge transfer from photoexcited molecules into the metal.

IV. CONCLUSIONS

Applying time-resolved PL spectroscopy to well-defined layered PTCDA films with systematically varying thickness, we are able to access the exciton lifetimes within individual molecular layers in these films. By that means, we identify the relaxation processes which underlie the decays of the prominent E and Y PL bands of PTCDA in the presence of the two different metal surfaces Ag(111) and Au(111).

Decay of the E emission, which corresponds to excimers or self-trapped excitons, can be explained with a surface-damping model, which implies these excitations localized at specific sites within the PTCDA films. Moreover, the efficiency of exciton quenching as a function of the molecule–metal distance is strongly affected by the particular metal substrate. This effect is explained within the framework of surface-damping as well, indicating that intraband transitions in the metal play an important role for the excitonic decay in PTCDA films on silver but are of less importance for PTCDA films deposited on gold.

For the Y emission, which is attributed to excitons with CT character, the luminescent lifetime is in general determined by a rather complex convolution of surface damping, diffusion along the PTCDA stacking direction, and exciton annihilation at the molecule/metal interface. Applying a hopping model to describe the diffusion of excitons through the molecular film, we reveal that in metal-supported PTCDA films the relaxation of CT excitons is largely determined by exciton diffusion and subsequent annihilation at the PTCDA/metal interface. Especially for thin films, the annihilation of excitons is drastically enhanced at the PTCDA/Ag(111) interface, which we attribute to the unoccupied metal–organic interface state of this system mediating charge transfer across the PTCDA/Ag(111) interface.

ACKNOWLEDGMENTS

The authors thank S. Chatterjee for helpful discussions and M. Koch for providing the streak camera. Funded by the Deutsche Forschungsgemeinschaft (DFG) through project SFB 1083.

[1] P. Fenter, F. Schreiber, L. Zhou, P. Eisenberger, and S. R. Forrest, Phys. Rev. B **56**, 3046 (1997).

[2] K. Glöckler, C. Seidel, A. Soukopp, M. Sokolowski, E. Umbach, M. Bohringer, R. Berndt, and W. D. Schneider, Surf. Sci. **405**, 1 (1998).

[3] E. Umbach, K. Glockler, and M. Sokolowski, Surf. Sci. **404**, 20 (1998).

[4] M. Leonhardt, O. Mager, and H. Port, Chem. Phys. Lett. **313**, 24 (1999).

[5] B. Krause, A. C. Dürr, K. Ritley, F. Schreiber, H. Dosch, and D. Smilgies, Phys. Rev. B **66**, 235404 (2002).

[6] L. Chkoda, M. Schneider, V. Shklover, L. Kilian, M. Sokolowski, C. Heske, and E. Umbach, Chem. Phys. Lett. **371**, 548 (2003).

[7] B. Krause, A. Dürr, F. Schreiber, H. Dosch, and O. Seeck, Surf. Sci. **572**, 385 (2004).

[8] L. Kilian, E. Umbach, and M. Sokolowski, Surf. Sci. **573**, 359 (2004).

[9] A. Hauschild, K. Karki, B. C. C. Cowie, M. Rohlfing, F. S. Tautz, and M. Sokolowski, Phys. Rev. Lett. **94**, 036106 (2005).

[10] F. S. Tautz, Prog. Surf. Sci. **82**, 479 (2007).

[11] C. H. Schwalb, S. Sachs, M. Marks, A. Schöll, F. Reinert, E. Umbach, and U. Höfer, Phys. Rev. Lett. **101**, 146801 (2008).

[12] A. Hauschild, R. Temirov, S. Soubatch, O. Bauer, A. Schöll, B. C. C. Cowie, T. L. Lee, F. S. Tautz, and M. Sokolowski, Phys. Rev. B **81**, 125432 (2010).

[13] M. Schneider, E. Umbach, and M. Sokolowski, Chem. Phys. **325**, 185 (2006).

[14] H. Marchetto, T. Schmidt, U. Groh, F. C. Maier, P. L. Lévesque, R. H. Fink, H.-J. Freund, and E. Umbach, Phys. Chem. Chem. Phys **17**, 29150 (2015).

[15] N. Armbrust, F. Schiller, J. Güdde, and U. Höfer, Sci. Rep. **7**, 46561 (2017).

[16] M. Hoffmann, K. Schmidt, T. Fritz, T. Hasche, V. M. Agranovich, and K. Leo, Chem. Phys. **258**, 73 (2000).

[17] V. M. Agranovich and A. A. Zakhidov, Chem. Phys. Lett. **50**, 278 (1977).

[18] V. Bulovic, P. E. Burrows, S. R. Forrest, J. A. Cronin, and M. E. Thompson, Chem. Phys. **210**, 1 (1996).

[19] H. P. Wagner, A. DeSilva, and T. U. Kampen, Phys. Rev. B **70**, 235201 (2004).

[20] W. Gebauer, A. Langner, M. Schneider, M. Sokolowski, and E. Umbach, Phys. Rev. B **69**, 155431 (2004).

[21] V. R. Gangilenka, L. V. Titova, L. M. Smith, H. P. Wagner, L. A. A. DeSilva, L. Gisslen, and R. Scholz, Phys. Rev. B **81**, 155208 (2010).

[22] U. Gómez, M. Leonhardt, H. Port, and H. Wolf, Chem. Phys. Lett. **268**, 1 (1997).

[23] A. Y. Kobitski, R. Scholz, I. Vragovic, H. P. Wagner, and D. R. T. Zahn, Phys. Rev. B **66**, 153204 (2002).

[24] A. Y. Kobitski, R. Scholz, D. R. T. Zahn, and H. P. Wagner, Phys. Rev. B **68**, 155201 (2003).

[25] C. H. Schwalb, M. Marks, S. Sachs, A. Schöll, F. Reinert, E. Umbach, and U. Höfer, Eur. Phys. J. B **75**, 23 (2010).

[26] S. Mannsfeld, M. Toerker, T. Schmitz-Hübsch, F. Sellam, T. Fritz, and K. Leo, Org. Electron. **2**, 121 (2001).

[27] M. Müller, A. Paulheim, A. Eisfeld, and M. Sokolowski, J. Chem. Phys. **139**, 044302 (2013).

[28] H. Proehl, R. Nitsche, T. Dienel, K. Leo, and T. Fritz, Phys. Rev. B **71**, 165207 (2005).

[29] M. Marks, C. H. Schwalb, S. Sachs, A. Schöll, and U. Höfer, J. Chem. Phys. **139**, 124701 (2013).

[30] B. Krause, A. Dürr, F. Schreiber, H. Dosch, and O. Seeck, J. Chem. Phys. **119**, 3429 (2003).

[31] R. Kaiser, M. Friedrich, T. Schmitz-Hübsch, F. Sellam, T. U. Kampen, K. Leo, and D. R. T. Zahn, Fresenius' J. Anal. Chem. **363**, 189 (1999).

[32] The stated SPP energies are the resonance energies of the surface loss function $\mathrm{Im}[(-1)/(1+\epsilon(\omega))]$ calculated with the dielectric functions of silver and gold, respectively, from Ref. [38].

[33] H. Proehl, T. Dienel, R. Nitsche, and T. Fritz, Phys. Rev. Lett. **93**, 097403 (2004).

[34] D. Schlettwein, A. Back, B. Schilling, T. Fritz, and N. Armstrong, Chem. Mater. **10**, 601 (1998).

[35] R. R. Chance, A. Prock, and R. Silbey, J. Chem. Phys. **60**, 2744 (1974).

[36] A. P. Alivisatos, D. H. Waldeck, and C. B. Harris, J. Chem. Phys. **82**, 541 (1985).

[37] G. Ford and W. Weber, Phys. Rep. **113**, 195 (1984).

[38] S. Babar and J. H. Weaver, Appl. Opt. **54**, 477 (2015).

[39] N. W. Ashcroft and N. D. Mermin, *Solid State Physics* (Hartcourt College Publishers, New York, 1976).

[40] M. Möbus, N. Karl, and T. Kobayashi, J. Cryst. Growth **116**, 495 (1992).

[41] S. K. M. Henze, O. Bauer, T. L. Lee, M. Sokolowski, and F. S. Tautz, Surf. Sci. **601**, 1566 (2007).

[42] R. Schuppel, T. Dienel, K. Leo, and M. Hoffmann, J. Lumin. **110**, 309 (2004).

[43] E. Engel, K. Leo, and M. Hoffmann, Chem. Phys. **325**, 170 (2006).